A Practical One-Shot Multispectral Imaging System Using a Single Image Sensor

Yusuke Monno, *Member, IEEE,* Sunao Kikuchi, Masayuki Tanaka, *Member, IEEE,* and Masatoshi Okutomi, *Member, IEEE*

Abstract—Single-sensor imaging using the Bayer color filter array (CFA) and demosaicking is well established for current compact and low-cost color digital cameras. An extension from the CFA to a multispectral filter array (MSFA) enables us to acquire a multispectral image in one shot without increased size or cost. However, multispectral demosaicking for the MSFA has been a challenging problem because of very sparse sampling of each spectral band in the MSFA. In this paper, we propose a high-performance multispectral demosaicking algorithm, and at the same time, a novel MSFA pattern that is suitable for our proposed algorithm. Our key idea is the use of the guided filter (GF) to interpolate each spectral band. To generate an effective guide image, in our proposed MSFA pattern, (i) we maintain the sampling density of the G band as high as the Bayer CFA, and (ii) we array each spectral band so that an adaptive kernel can be estimated directly from raw MSFA data. Given these two advantages, we effectively generate the guide image from the most densely sampled G band using the adaptive kernel. In experiments, we demonstrate that our proposed algorithm with our proposed MSFA pattern outperforms existing algorithms and provides better color fidelity compared with a conventional color imaging system with the Bayer CFA. We also show some real applications using a multispectral camera prototype we built.

Index Terms—Demosaicking, interpolation, multispectral filter array (MSFA), multispectral imaging, guided filter.

I. INTRODUCTION

THE energy of light emitted from light sources or reflected by objects continuously spans a wide range of wavelengths. In typical color imaging, only three spectral bands (R, G, and B bands) are measured. For this reason, a considerable amount of potentially available spectral information is lost. In contrast, multispectral imaging with more than three spectral bands can offer reliable spectral information about a captured scene, which is very useful for many computer vision and image processing applications including digital archives [1], high-fidelity color reproduction [2], relighting [3], segmentation [4], and tracking [5].

In the past few decades, many multispectral imaging systems have been proposed [2]–[11] (see [12] for a comprehensive review). However, in practical use, these systems present limitations of size, cost, and real-time processing because of the requirement of multiple cameras [2], [5], [6], multiple shots [7], [8], a high-speed lighting system [3], [9], or a

Y. Monno, M. Tanaka, and M. Okutomi are with the Department of Mechanical and Control Engineering, Tokyo Institute of Technology, Meguro-ku, Tokyo, 152-8550, Japan (e-mail: ymonno@ok.ctrl.titech.ac.jp; mtanaka@ctrl.titech.ac.jp; mxo@ctrl.titech.ac.jp).

S. Kikuchi is with the Olympus R&D Center, Hachioji-shi, Tokyo, 192-8512, Japan (e-mail: sunao_kikuchi@ot.olympus.co.jp).

special optical element such as a prism and a diffraction grating [4], [5], [10], [11]. In contrast, single-sensor imaging with the Bayer color filter array (CFA) [13] and demosaicking is well established for current compact and low-cost color digital cameras [14], where only one pixel value among RGB values is recorded at each pixel location because of spatial subsampling of the RGB bands by the CFA. The acquired mosaic data is called raw CFA data. A full-color image is generated from the raw CFA data by an interpolation process called demosaicking [15]–[17]. This single-sensor technology enables us to capture a color image in one shot and a color video in real time.

One solution for practical multispectral imaging is an extension from the CFA to a multispectral filter array (MSFA) [18]–[24], which enables us to acquire a multispectral video in real time without increased size and cost. In the MSFA, more than three spectral bands are arrayed. However, the extension from the CFA to the MSFA is not straightforward because of the following challenges: (i) multispectral demosaicking for the MSFA is a challenging problem because of very sparse sampling of each spectral band in the MSFA caused by the increase of arrayed spectral bands, (ii) we have to design not only the demosaicking algorithm but also an MSFA pattern because of the absence of a de-facto standard MSFA pattern corresponding to the Bayer pattern for the RGB color imaging, and (iii) we also have to consider the feasibility of the demosaicking algorithm and the MSFA pattern in a real hardware setup.

Although many sophisticated demosaicking algorithms have been proposed for the Bayer CFA [15]–[17], not many studies have addressed the multispectral demosaicking and the design of the MSFA pattern. Existing multispectral demosaicking algorithms merely apply a classical demosaicking algorithm such as edge-sensing interpolation [18], [19], bilinear interpolation of color differences [20], median filtering [21], or linear demosaicking [22], [23]. These classical algorithms are easily extensible for the MSFA, but their performance is insufficient. The demosaicking performance also depends on the MSFA pattern. However, most existing works have not examined which MSFA pattern is better for the demosaicking algorithm. In addition, the existing works, including our previous works [25], [26], are only theoretical ones and have not tested their feasibility in a real hardware setup.

In this paper, we propose a high-performance multispectral demosaicking algorithm, and at the same time, a novel MSFA pattern suitable for the proposed demosaicking algorithm. In our proposed algorithm, we interpolate each subsampled

spectral band by the guided filter (GF) [27], which is a high-performance edge-preserving filter. The key to high-performance interpolation by the GF is to obtain an effective guide image that preserves edges and textures. With this key in mind, we design our proposed MSFA pattern based on a generic method [18] to have two desirable properties for generating the effective guide image from raw MSFA data. In experiments, we demonstrate that (i) our joint design of the demosaicking algorithm and the MSFA pattern significantly improves the demosaicking accuracy and (ii) our proposed algorithm with our proposed MSFA pattern outperforms existing algorithms and provides better color fidelity compared with a conventional color imaging system with the Bayer CFA. Not only theoretical study, we also show some real applications using a one-shot multispectral camera prototype we built.

The remainder of this paper is organized as follows. In Section II, we present a short review of existing single-sensor imaging systems. We describe our joint design of the demosaicking algorithm and the MSFA pattern in Section III. Experimental results are reported in Section IV. The configuration of our multispectral camera prototype and its applications are reported in Section V. Finally, conclusion is presented in Section VI.

II. RELATED WORKS

Classifying by filter types, we briefly review previously proposed single-sensor imaging systems.

RGB filters The most popular and widely used CFA is the Bayer CFA [13], for which numerous demosaicking algorithms have been proposed [15]–[17]. Although current state-of-the-art Bayer demosaicking algorithms [28]–[31] can offer superior performance, these algorithms are specially designed for the Bayer CFA. The CFAs alternative to the Bayer CFA have also been proposed [32]–[34]. Universal demosaicking algorithms for these CFAs have also been developed [35], [36]. However, these universal algorithms are only applicable for the CFAs with RGB primary filters.

Linear combination of RGB filters Recently, some CFAs with multiple color filters have been proposed [37], [38]. In these CFAs, each color filter consists of a linear combination of the RGB primary filters as below:

$$S_c(\lambda) = \alpha S_r(\lambda) + \beta S_g(\lambda) + \gamma S_b(\lambda), \quad (1)$$

where $S_c(\lambda)$ is the resultant filter sensitivity at the wavelength λ, which is a linear combination of the sensitivities of the RGB primary filters, $S_r(\lambda)$, $S_g(\lambda)$, and $S_b(\lambda)$. Demosaicking algorithms for an arbitrary CFA including the above CFAs have also been proposed [39], [40]. Because each color filter is designed as a linear combination of the RGB primary filters, these works are not beyond the scope of three-band color imaging. Also, it is physically infeasible to develop such color filters.

RGB-White filters Some CFAs contain RGB pixels plus white (panchromatic) pixels [41]–[43]. The purpose of these CFAs is to improve the sensor sensitivity, rather than to acquire multispectral information. Most demosaicking algorithms for these CFAs apply simple color difference interpolation [42] or linear demosaicking [43].

RGB-NIR filters A special category of the MSFAs is an MSFA designed for simultaneous capturing of RGB and near-infrared (NIR) images [44]–[46]. In [44], [45], the authors simultaneously optimized the MSFA (more specifically, optimized a combination ratio of the RGB and NIR filters to form each spectral filter) and a linear demosaicking matrix by describing the whole imaging system in a linear form. This approach can be generalized for multispectral imaging in theory. However, as mentioned before, it is physically infeasible to develop spectral filters described as a linear combination of other filters. In [46], the authors proposed a demosaicking algorithm to generate a high-quality RGB image and one additional band image, typically NIR image. However, it is not straightforward to extend the algorithm for multispectral imaging with more than four spectral bands.

Multispectral filters Brauers and Aach proposed an MSFA with six evenly subsampled narrow-band filters [20]. Yasuma et al. proposed a generalized assorted pixel mosaic that can capture a seven-band image [22]. Aggarwal and Majumdar proposed a framework to design uniform MSFAs [23]. In these works, simple demosaicking algorithms such as bilinear interpolation of color differences [20], median filtering [21], and linear demosaicking [22], [23] are applied. Although these simple algorithms are easily extensible for the MSFA, their performance is insufficient. As another approach, Baone and Qi proposed a maximum a posteriori probability (MAP)-based demosaicking algorithm [24]. However, the MAP-based algorithm is not practical because it necessarily entails high computational cost.

The most closely related works to the study described in this paper are those of Miao et al. [18], [19]. Miao and Qi proposed a generic method for generating MSFA patterns [18]. By recursively separating checkerboard patterns, the generic method generates the MSFA pattern given the number of spectral bands and the sampling densities of each spectral band. Several works follow this method to develop a demosaicking algorithm [21], [24]. Miao et al. also proposed the binary tree-based edge-sensing (BTES) demosaicking algorithm [19], which is applicable for all the MSFA patterns that can be generated by the generic method [18]. The BTES algorithm iteratively performs edge-sensing interpolation to generate a full multispectral image. Although the generic method and the BTES algorithm are useful as a general framework, the performance of the BTES algorithm is insufficient for severely undersampled raw MSFA data. Additionally, in the generic method, the authors have not discussed which MSFA pattern among possible patterns is the best for the BTES algorithm.

Finally, all the works mentioned in this category are not beyond theoretical ones and have not tested their feasibility in a real hardware setup.

III. JOINT DESIGN OF MSFA PATTERN AND DEMOSAICKING ALGORITHM

Fig. 1 (a) shows our proposed MSFA pattern. Fig. 1 (b) shows the corresponding spectral sensitivities of each spectral band. In this paper, we examine the design of a five-band MSFA and call the spectral bands R, Or, G, Cy,
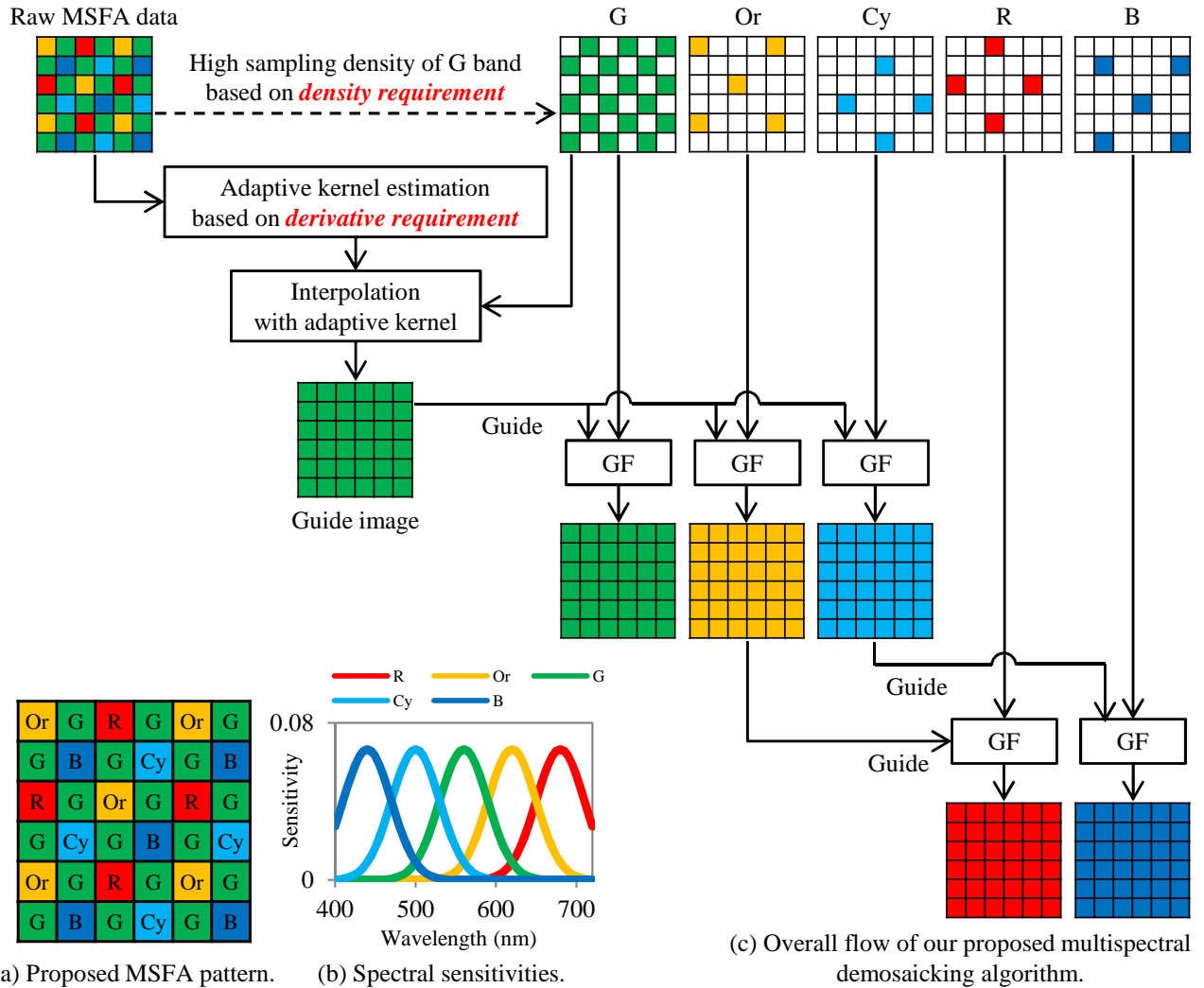
Fig. 1. (a) Our proposed MSFA pattern, (b) spectral sensitivities of each spectral band, and (c) the overall flow of our proposed multispectral demosaicking algorithm. In our proposed algorithm, we first generate the guide image for the GF from the most densely sampled G band by the interpolation with an adaptive kernel. The adaptive kernel is estimated from raw MSFA data based on the derivative requirement. Then, the GF is performed to interpolate the G, Or, and Cy bands. For the interpolation of the R and B bands, we update the guide image to the interpolated Or and Cy band images respectively.

and B bands respectively from the long-wavelength end to the short-wavelength end. For the spectral sensitivities, we simply assume uniform Gaussian sensitivities. Generally, in multispectral imaging, an increasing number of spectral bands is expected to improve spectral estimation accuracy [47], [48]. However, it is not necessarily true for the single-sensor multispectral imaging because sampling densities of each spectral band in the MSFA become lower if we array more spectral bands. Therefore, there is a trade-off between the number of spectral bands and the spatial resolution. It is also known that the demosaicking performance is affected by the spectral sensitivities [49]–[52]. Although all of these components should be considered together, the investigation of optimal spectral number and spectral sensitivities is beyond the scope of this paper and our future work. Hereafter, we describe the MSFA pattern as the MSFA for simple notation.

Fig. 1 (c) shows the overall flow of our proposed multispectral demosaicking algorithm. Our key idea is to use the GF [27] to interpolate each spectral band. In the GF, the guide image quality plays a crucial role for high-performance interpolation. To generate the guide image effectively, we select our proposed MSFA based on two design requirements: (i) *Density requirement*; we maintain the sampling density of the G band as high as the Bayer CFA, and (ii) *Derivative requirement*; we array each spectral band so that derivatives can be calculated at every pixel location from raw MSFA data using our proposed derivative calculation method. In our algorithm, we first generate the effective guide image from the most densely sampled G band by the interpolation with an adaptive kernel, which is estimated based on the calculated derivatives from raw MSFA data. Then, we interpolate the G, Or, and Cy bands by the GF using the generated guide image assuming spectral correlations. For the interpolation of the R and B bands, we respectively update the guide image to the interpolated Or and Cy band images because closer spectral bands have a higher spectral correlation.

TABLE I
THE PROPERTIES OF THE THREE MSFA PATTERNS SHOWN IN FIG. 2.

	MSFA1	MSFA2	Proposed MSFA
Sampling densities $\{G, Or, Cy, R, B\}$	$\{\frac{1}{4}, \frac{1}{4}, \frac{1}{4}, \frac{1}{8}, \frac{1}{8}\}$	$\{\frac{1}{2}, \frac{1}{4}, \frac{1}{8}, \frac{1}{16}, \frac{1}{16}\}$	$\{\frac{1}{2}, \frac{1}{8}, \frac{1}{8}, \frac{1}{8}, \frac{1}{8}\}$
Density requirement		✓	✓
Derivative requirement	✓		✓

(a) Binary tree for MSFA1

(b) Binary tree for MSFA2

(c) Binary tree for our proposed MSFA

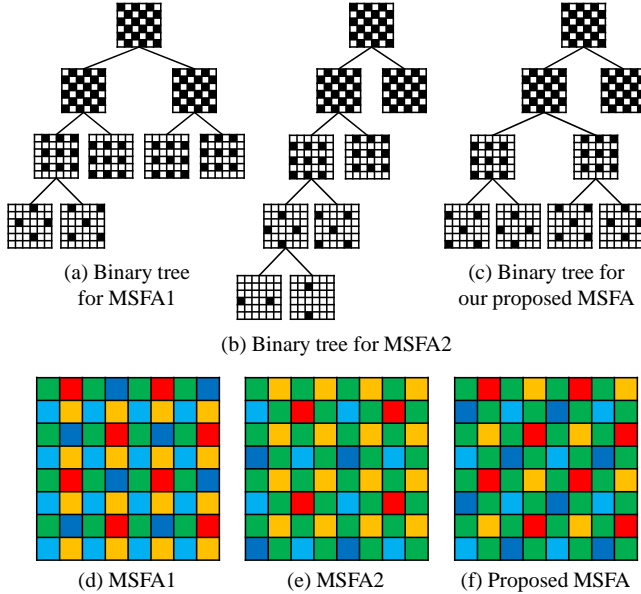(d) MSFA1   (e) MSFA2   (f) Proposed MSFA

Fig. 2. (a)-(c) Three possible binary trees for a five-band MSFA generated by the generic method and (d)-(f) the resultant three MSFAs generated from each binary tree by assigning higher sampling densities in the order of G, Or, Cy, R, and B bands. (f) is our proposed MSFA.

Diagonal derivatives at Or pixel

$$z_u(m,n) = I^{cy}_{m-1,n+1} - I^{cy}_{m+1,n-1}$$

$$z_v(m,n) = I^{b}_{m-1,n-1} - I^{b}_{m+1,n+1}$$

Diagonal derivatives at Cy pixel

$$z_u(m,n) = I^{or}_{m-1,n+1} - I^{or}_{m+1,n-1}$$

$$z_v(m,n) = I^{r}_{m-1,n-1} - I^{r}_{m+1,n+1}$$

Fig. 3. Examples of the diagonal derivative calculation at Or and Cy pixel locations.

A. Selection of our proposed MSFA

We select our proposed MSFA from candidate MSFAs generated by the generic method [18] based on the density requirement and the derivative requirement. The generic method generate the MSFAs by recursively separating the checkerboard pattern based on a binary tree. The binary tree is defined by the number of spectral bands and the sampling densities of each spectral band, which are given by users. Fig. 2 (a)-(c) show the three possible binary trees for a five-band MSFA. The MSFA is formed by assigning each spectral band to a leaf of the binary tree. Because it is not impractical to compare all assigning combinations for each binary tree, we here assign higher sampling densities in the order of G, Or, Cy, R, and B bands considering our proposed demosaicking algorithm assuming spectral correlations and the guide update strategy. Fig. 2 (d)-(f) show the resultant three MSFAs including our proposed MSFA (Fig. 2 (f)). We describe the other two MSFAs as MSFA1 and MSFA2 respectively.

In the density requirement, we maintain the sampling density of the G band as high as the Bayer CFA to make the interpolation for the guide image precise. In the derivative requirement, we calculate derivatives at every pixel location from raw MSFA data. Almost all existing interpolation algorithms seek to exploit the derivatives (also called gradients) to interpolate the input data along edge directions. However, we
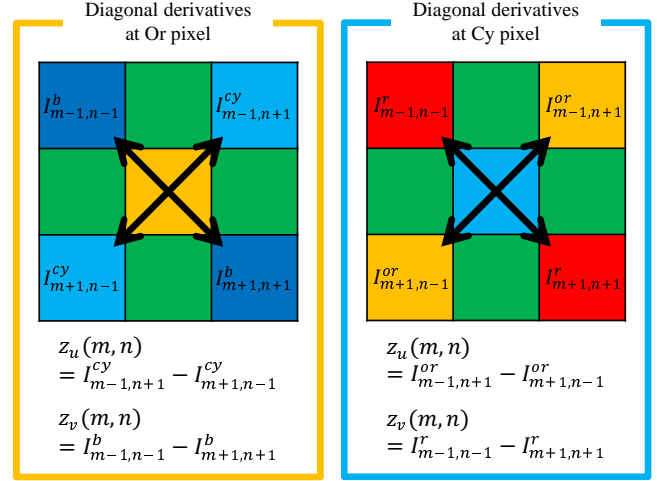
usually cannot calculate the derivatives directly from the raw MSFA data because different spectral bands are arrayed in a mosaic pattern. Here, we propose a novel derivative calculation method from raw MSFA data.

For natural images, spectral bands are well known to be correlated in high-frequency components [53]. Based on this fact, we assume that the derivatives of each spectral band are approximately equivalent. Then, we calculate the derivatives in diagonal directions as

$$z_u(m,n) = I^{c_u}_{m-1,n+1} - I^{c_u}_{m+1,n-1}, \tag{2}$$

$$z_v(m,n) = I^{c_v}_{m-1,n-1} - I^{c_v}_{m+1,n+1}, \tag{3}$$

where z_u and z_v are the diagonal derivatives at a pixel location (m,n), $I^{c}_{m,n}$ is a pixel intensity of the c band at the pixel location (m,n), and c_u and c_v are corresponding spectral bands at respective pixel locations. Fig. 3 shows examples of the diagonal derivative calculation at Or and Cy pixel locations in our proposed MSFA. In this way, we calculate the derivatives in the diagonal directions, instead of the standard horizontal and vertical directions because it is impossible to array each spectral band to calculate horizontal and vertical derivatives by the similar way for any five-band MSFA. As a consequence of our proposed derivative calculation method, the derivative requirement is that all pixels must have adjacent diagonal pixels of the same spectral band in each diagonal direction.

Table I presents a summary of the properties that each MSFA has. Consequently, only our proposed MSFA satisfies both the density requirement and the derivative requirement.

B. Proposed multispectral demosaicking algorithm

In our proposed algorithm, we first generate the guide image for the GF by interpolating the G band using an adaptive kernel. The adaptive kernel is a spatially variant kernel estimated based on image structures, which is adaptive to edges and textures [54]. We estimate the adaptive kernel in a similar way with the original method [54] as

$$k_{\mathbf{x}_p}(\mathbf{x}) = \exp\left[-\frac{\mathbf{x}^T \mathbf{H}^T \mathbf{C}_{\mathbf{x}_p}^{-1} \mathbf{H}\mathbf{x}}{2h^2 \mu_{\mathbf{x}_p}{}^2}\right], \tag{4}$$

where $\mathbf{C}_{\mathbf{x}_p}$ is the covariance matrix of the Gaussian kernel, h stands for a global smoothing parameter, $\mu_{\mathbf{x}_p}$ is a local smoothing parameter, which controls the kernel size at each pixel location, and $\mathbf{H}$ is a rotation matrix that aligns the pixel coordinates with the direction of the derivatives. Specifically, we use the rotation matrix, which rotates the pixel coordinates by 45 degrees. The covariance matrix $\mathbf{C}_{\mathbf{x}_p}$ is estimated based on the diagonal derivatives around the location $\mathbf{x}_p$ as

$$\mathbf{C}_{\mathbf{x}_p}^{-1} = \frac{1}{|N_{\mathbf{x}_p}|}$$
$$\begin{pmatrix} \sum\limits_{\mathbf{x}_j \in N_{\mathbf{x}_p}} z_u(\mathbf{x}_j)z_u(\mathbf{x}_j) & \sum\limits_{\mathbf{x}_j \in N_{\mathbf{x}_p}} z_u(\mathbf{x}_j)z_v(\mathbf{x}_j) \\ \sum\limits_{\mathbf{x}_j \in N_{\mathbf{x}_p}} z_u(\mathbf{x}_j)z_v(\mathbf{x}_j) & \sum\limits_{\mathbf{x}_j \in N_{\mathbf{x}_p}} z_v(\mathbf{x}_j)z_v(\mathbf{x}_j) \end{pmatrix}, \tag{5}$$

where z_u and z_v are the diagonal derivatives calculated from the raw MSFA data, $N_{\mathbf{x}_p}$ denotes neighbor pixels around the location $\mathbf{x}_p$, and $|N_{\mathbf{x}_p}|$ is a normalizing factor, which is the number of pixels included in $N_{\mathbf{x}_p}$.

Based on the adaptive kernel weight, the guide image is interpolated as

$$I_{\mathbf{x}_p}^g = \frac{1}{W_{\mathbf{x}_p}} \sum_{\mathbf{x}_i \in \omega_{\mathbf{x}_p}} k_{\mathbf{x}_p}(\mathbf{x}_i - \mathbf{x}_p) M_{\mathbf{x}_i} I_{\mathbf{x}_i}^g, \tag{6}$$

where $I_{\mathbf{x}_p}^g$ stands for the interpolated G pixel value at the location $\mathbf{x}_p$, $M_{\mathbf{x}_i}$ signifies a binary mask at the location $\mathbf{x}_i$, $k_{\mathbf{x}_p}(\mathbf{x})$ denotes the adaptive kernel weight, $\omega_{\mathbf{x}_p}$ represents a window centered at the location $\mathbf{x}_p$, and $W_{\mathbf{x}_p}$ is a normalizing factor that is the sum of the kernel weights. The binary mask $M_{\mathbf{x}_i}$ is set to one if the G band data is sampled at the associated pixel location and zero for other cases.

Then, we interpolate each spectral band by the GF [27]. The generated G band guide image is used for interpolating the G, Or, and Cy bands[1]. For the interpolation of the R and B bands, we update the guide image to the interpolated Or and Cy band images respectively.

In the GF, the filter output in each local window is modeled by a linear transformation of the guide image as

$$q_{\mathbf{x}_i} = a_{\mathbf{x}_p} I_{\mathbf{x}_i} + b_{\mathbf{x}_p}, \quad \forall \mathbf{x}_i \in \omega_{\mathbf{x}_p}, \tag{7}$$

where $\omega_{\mathbf{x}_p}$ represents a window centered at the pixel location $\mathbf{x}_p$, $\mathbf{x}_i$ is a pixel location in the window, $q_{\mathbf{x}_i}$ is the filter output at the location $\mathbf{x}_i$, and $I_{\mathbf{x}_i}$ is the intensity of the guide image at the location $\mathbf{x}_i$. The linear coefficients $(a_{\mathbf{x}_p}, b_{\mathbf{x}_p})$ for each window are estimated by minimizing the following cost function:

$$E(a_{\mathbf{x}_p}, b_{\mathbf{x}_p}) = \sum_{\mathbf{x}_i \in \omega_{\mathbf{x}_p}} M_{\mathbf{x}_i}((a_{\mathbf{x}_p} I_{\mathbf{x}_i} + b_{\mathbf{x}_p} - p_{\mathbf{x}_i})^2 + \epsilon a_{\mathbf{x}_p}^2), \tag{8}$$

where $p_{\mathbf{x}_i}$ is the intensity of the input subsampled data at the location $\mathbf{x}_i$, $M_{\mathbf{x}_i}$ is the binary mask at the location $\mathbf{x}_i$, and ϵ is a smoothing parameter. Because the location $\mathbf{x}_i$ is involved in all windows that contain the location $\mathbf{x}_i$, the original GF generates the final output at the location $\mathbf{x}_i$ by simply averaging the results of each window. Instead, we introduce a weighting averaging based on the cost as

$$q_{\mathbf{x}_i} = \bar{a}_{\mathbf{x}_i} I_{\mathbf{x}_i} + \bar{b}_{\mathbf{x}_i}, \tag{9}$$

where

$$\bar{a}_{\mathbf{x}_i} = \frac{1}{W_{\mathbf{x}_i}} \sum_{\mathbf{x}_p \in \omega_{\mathbf{x}_i}} \exp\left(-\alpha E\left(a_{\mathbf{x}_p}, b_{\mathbf{x}_p}\right)\right) a_{\mathbf{x}_p}, \tag{10}$$

$$\bar{b}_{\mathbf{x}_i} = \frac{1}{W_{\mathbf{x}_i}} \sum_{\mathbf{x}_p \in \omega_{\mathbf{x}_i}} \exp\left(-\alpha E\left(a_{\mathbf{x}_p}, b_{\mathbf{x}_p}\right)\right) b_{\mathbf{x}_p}, \tag{11}$$

where α is a parameter that controls the weighting and $W_{\mathbf{x}_i}$ is the normalizing factor, which is the sum of the weights.

IV. EXPERIMENTAL RESULTS

A. Datasets and experimental settings

In experiments, we used two multispectral image datasets: the CAVE dataset [22], [56] and our dataset. Both datasets were captured using a monochrome camera with a Varispec liquid crystal tunable filter [7], [57]. The CAVE dataset consists of 31-band multispectral images of 32 scenes. The 31-band images are acquired at every 10 nm from 400nm to 700nm. The image size is 512×512. The CAVE dataset is often used as a standard multispectral image dataset. In the CAVE dataset, many images are dominated by smooth objects or backgrounds. Our dataset consists of 31-band images, which are acquired at every 10 nm from 420nm to 720nm[2]. The original image size of our 31-band images is 2048×2048. From the original high-resolution images, we generated clipped image dataset of 30 scenes as shown in Fig. 4. The image size of the clipped images is 500×500. We selected the clipped regions with rich textures and colorful objects. This is because the main challenges of the single-sensor multispectral imaging are in the texture and colorful regions. For smooth regions, demosaicking algorithms generally work well for both the three-band Bayer CFA and the proposed five-band MSFA. For colorless regions, both typical three-band imaging and our proposed five-band imaging can reproduce accurate colors.

Ground-truth five-band images were simulated from the 31-band images. Then, the mosaicking and demosaicking processes were performed. To evaluate colorimetric accuracy in the sRGB domain, we estimated spectral reflectance images from the demosaicked five-band images and converted the reflectance images to sRGB images using xyz color matching

---

[1]We also apply the GF to the G band because if a smoothing parameter $\epsilon \neq 0$ in Eq. (8), the result G band image is not identical to the guide image.

[2]We removed 400nm and 410nm because they are unreliable as a result of the very low sensitivities of the Varispec filter in 400nm and 410nm.

Fig. 4. Our multispectral image dataset.

TABLE II
THE AVERAGE PSNR, CPSNR, DeltaE, AND CIEDE2000 [55] PERFORMANCE OF DIFFERENT DEMOSAICKING ALGORITHMS AND MSFAs. THE VALUES IN PARENTHESES REPRESENT THE STANDARD DEVIATION.

Light	Data	MSFA pattern	Algo.	PSNR R	PSNR Or	PSNR G	PSNR Cy	PSNR B	5band PSNR Ave.	sRGB PSNR Ave.	CPSNR	DeltaE	CIEDE 2000
D65	CAVE	MSFA1	BTES	42.59 (4.43)	42.04 (4.29)	40.90 (4.22)	40.28 (4.41)	40.54 (4.72)	41.27 (4.25)	36.63 (3.88)	36.43 (3.87)	2.67 (1.07)	3.54 (1.14)
			Proposed	44.70 (5.02)	42.92 (5.00)	41.43 (4.20)	41.27 (4.71)	41.78 (4.97)	42.42 (4.59)	37.42 (4.05)	37.24 (4.06)	2.52 (1.01)	3.33 (1.01)
		MSFA2	BTES	39.26 (4.11)	42.11 (4.32)	46.54 (4.42)	37.84 (4.35)	37.30 (4.47)	40.61 (4.16)	36.83 (3.84)	35.61 (3.86)	2.92 (1.15)	3.76 (1.15)
			Proposed	43.59 (4.62)	**45.02** (4.57)	45.71 (4.25)	43.09 (5.00)	41.81 (4.83)	43.85 (4.49)	39.08 (3.94)	38.65 (3.98)	2.44 (0.93)	3.20 (0.84)
		Proposed	BTES	42.60 (4.45)	39.41 (4.21)	46.54 (4.42)	37.83 (4.31)	40.46 (4.70)	41.37 (4.26)	36.94 (3.83)	35.81 (3.87)	2.85 (1.17)	3.81 (1.25)
			Proposed	**45.36** (4.49)	44.76 (4.70)	**48.06** (4.80)	**44.68** (4.86)	**43.96** (4.82)	**45.36** (4.56)	**40.00** (3.86)	**39.38** (3.89)	**2.35** (0.95)	**3.09** (0.87)
D65	Our	MSFA1	BTES	38.30 (3.99)	40.84 (4.27)	39.72 (4.50)	40.14 (4.80)	39.24 (4.30)	39.65 (4.15)	35.79 (3.57)	35.41 (3.52)	1.86 (0.55)	2.31 (0.70)
			Proposed	42.17 (4.94)	41.30 (5.05)	40.34 (4.60)	40.49 (4.87)	42.12 (4.86)	41.28 (4.56)	36.74 (3.82)	36.19 (3.75)	1.78 (0.55)	2.20 (0.69)
		MSFA2	BTES	34.71 (3.60)	40.81 (4.14)	45.51 (5.00)	36.31 (4.58)	35.49 (3.97)	38.57 (3.97)	35.40 (3.48)	34.10 (3.45)	2.31 (0.72)	2.74 (0.88)
			Proposed	42.28 (4.89)	**43.83** (4.97)	44.63 (4.66)	42.03 (4.92)	41.99 (4.73)	42.95 (4.47)	38.34 (3.76)	37.75 (3.67)	1.68 (0.53)	2.05 (0.64)
		Proposed	BTES	38.27 (3.94)	37.05 (4.01)	45.51 (5.00)	36.34 (4.57)	39.11 (4.27)	39.26 (4.09)	35.58 (3.59)	34.28 (3.46)	2.07 (0.63)	2.58 (0.83)
			Proposed	**43.82** (5.41)	43.28 (5.61)	**46.57** (5.99)	42.92 (5.20)	**43.62** (5.19)	**44.04** (5.09)	**39.00** (4.02)	**38.07** (3.92)	**1.56** (0.52)	**1.88** (0.61)

functions and the xyz to sRGB transformation matrix with a correct white point [58], [59]. We used a linear model based spectral reflectance estimation method [3], [9] with eight spectral basis functions and the regularization parameter = 0.1. The spectral basis functions were calculated using PCA from 1269 Munsell color samples [60]. We used the CIE A (incandescence), CIE D65 (daylight), and CIE F12 (fluorescent) illuminants [58], [59] for the evaluation. We evaluated the PSNR, CPSNR, DeltaE (Euclidean distance in Lab space), and CIEDE2000 [55] performance for numerical evaluation.

For our proposed algorithm, we used the smoothing parameters $h = 1/255$ and $\mu_{\mathbf{x}_p} = 1$ in Eq. (4), the 7×7 window for the covariance matrix estimation in Eq. (5), the 3×3 window for guide image generation in Eq. (6), the 9×9 window for the GF and the smoothing parameter $\epsilon = 0$ in Eq. (8), and the weighting parameter $\alpha = 3000$ in Eq. (10) and Eq. (11). Pixel intensities were normalized from 0 to 1 in all processes.

B. Comparison of multispectral demosaicking algorithms for different MSFAs

We first compare our proposed algorithm with the BTES algorithm [19] for the three MSFAs shown in Fig. 2. Table II presents the numerical performance of the algorithms for the three MSFAs under the CIE D65 illuminant. Our proposed algorithm with our proposed MSFA generally provides superior results. For the Or band, the MSFA2 outperforms ours because the MSFA2 has the higher sampling density of the Or band in addition to the high sampling density of the G band. Fig. 5 shows a visual comparison[3] of the guide images generated using our proposed algorithm for the three MSFAs. The MSFA2 only satisfies the density requirement. We performed simple edge-sensing interpolation to generate the guide image because the adaptive kernel is not available. Consequently, severe artifacts arise in edges. The MSFA1 only satisfies

[3]Gamma correction is applied merely for display in all result images in this paper.
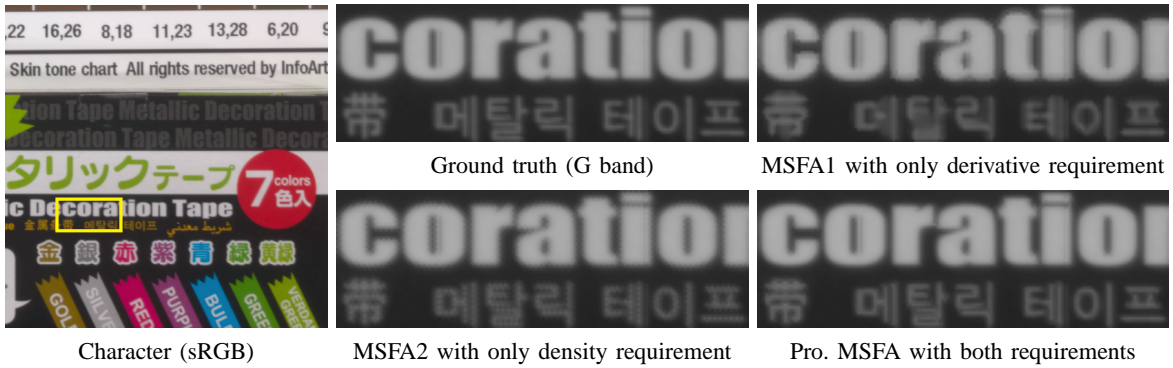
Ground truth (G band)   MSFA1 with only derivative requirement

Character (sRGB)   MSFA2 with only density requirement   Pro. MSFA with both requirements

Fig. 5. Visual comparison of the guide images generated by our proposed algorithm using different MSFAs.

CAVE dataset:
Egyptian statue (sRGB)

Ground truth (Cy band)

MSFA1 + BTES   MSFA2 + BTES   Pro. MSFA + BTES

MSFA1 + Pro. Algo.   MSFA2 + Pro. Algo.   Pro. MSFA + Pro. Algo.

Our dataset:
Can (sRGB)

Ground truth (R band)

MSFA1 + BTES   MSFA2 + BTES   Pro. MSFA + BTES

MSFA1 + Pro. Algo.   MSFA2 + Pro. Algo.   Pro. MSFA + Pro. Algo.
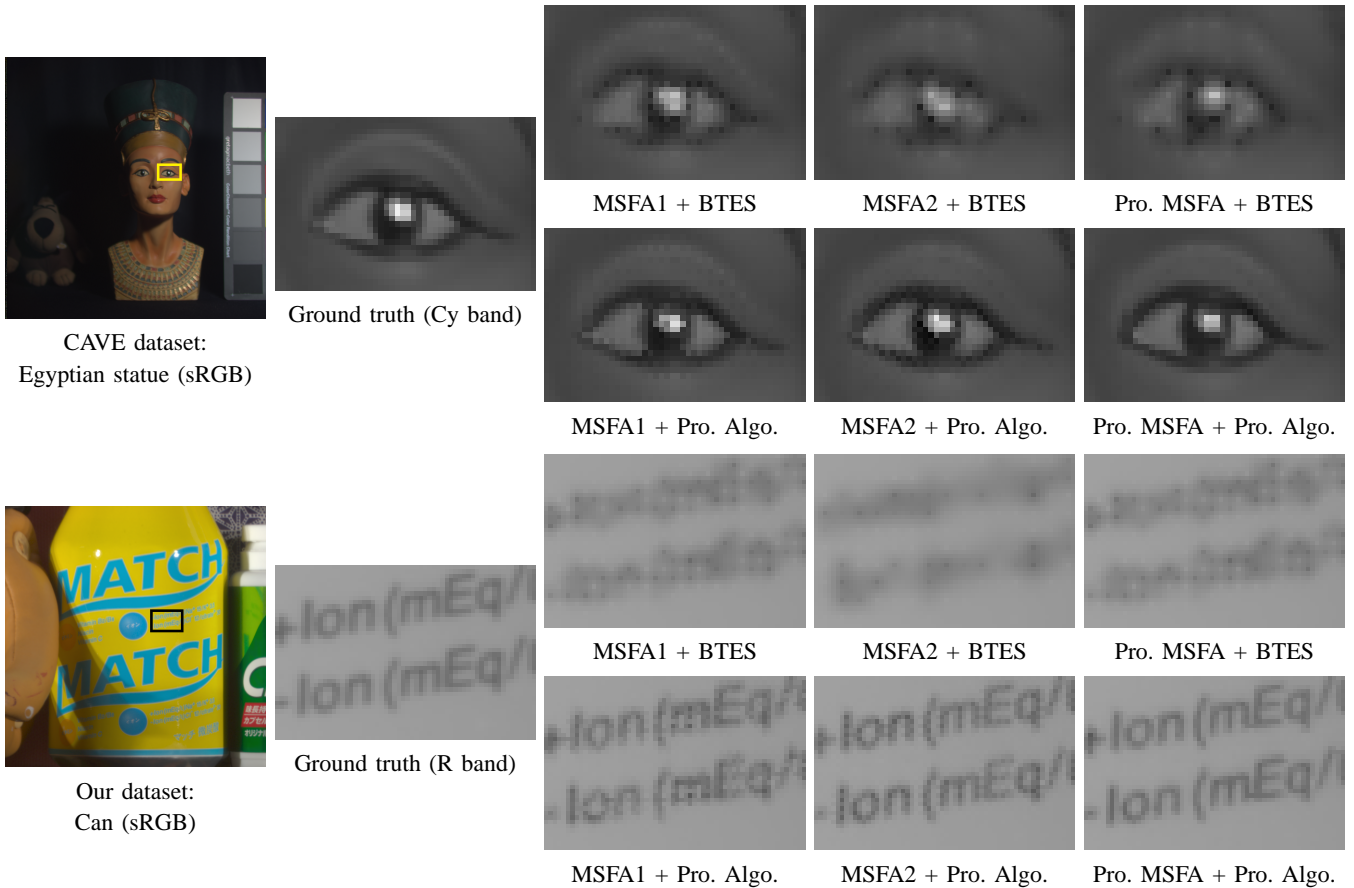
Fig. 6. Visual comparison of the demosaicked images using different MSFAs and demosaicking algorithms.

the derivative requirement. Compared with the MSFA1, the artifacts in edges are reduced because the adaptive kernel is useful for the guide image generation. However, the result guide image is blurred because of the low sampling density of the G band. In contrast, our proposed MSFA satisfies the both requirements. The guide image is effectively generated from the G band with the high-sampling density using the adaptive kernel. Fig. 6 shows a visual comparison of the demosaicked images. These results demonstrate the effectiveness of our joint design of the MSFA and demosaicking algorithm, which markedly improves the demosaicking performance.

C. Comparison of multispectral imaging with color imaging

We next compare the five-band multispectral imaging with the conventional three-band color imaging using the Bayer CFA. For the three-band Bayer CFA, the similar process flow as the five-band MSFA was simulated to generate the sRGB images, assuming the spectral sensitivities of a real color camera. We used the adaptive homogeneity-directed (AHD) algorithm [28] and the local polynomial approximation (LPA) algorithm [29] for the Bayer demosaicking. Both algorithms are well known high-performance Bayer demosaicking algorithms.

Table III presents a summary of numerical performance

TABLE III
THE AVERAGE PSNR, CPSNR, DELTAE AND CIEDE2000 [55] PERFORMANCE OF THE CONVENTIONAL COLOR IMAGING WITH THE BAYER CFA AND THE FIVE-BAND MULTISPECTRAL IMAGING. FOR THE BTES ALGORITHM, WE SELECTED THE BEST MSFA (MSFA1) IN TERMS OF THE CIEDE2000 METRIC IN TABLE II. THE VALUES IN PARENTHESIS REPRESENT THE STANDARD DEVIATION.

Light	Data	MSFA pattern	Algo.	PSNR R	PSNR Or	PSNR G	PSNR Cy	PSNR B	5band PSNR Ave.	sRGB PSNR Ave.	CPSNR	DeltaE	CIEDE 2000
A	CAVE	Bayer	AHD	-	-	-	-	-	-	36.60 (3.66)	31.59 (3.64)	2.49 (1.24)	2.55 (0.97)
		Bayer	LPA	-	-	-	-	-	-	37.46 (3.54)	32.61 (3.54)	2.31 (1.07)	2.46 (0.91)
		MSFA1	BTES	39.98 (4.44)	42.25 (4.33)	45.20 (4.18)	49.59 (4.30)	54.48 (4.59)	46.30 (4.21)	36.34 (3.84)	35.48 (3.74)	1.91 (0.86)	2.49 (1.03)
		Proposed	Proposed	**43.00** (4.42)	**45.04** (4.60)	**52.39** (4.73)	**54.13** (4.88)	**59.15** (4.74)	**50.74** (4.51)	**39.98** (3.83)	**38.52** (3.76)	**1.71** (0.73)	**2.19** (0.84)
A	Our	Bayer	AHD	-	-	-	-	-	-	33.36 (3.71)	27.58 (3.90)	3.29 (1.30)	2.62 (0.87)
		Bayer	LPA	-	-	-	-	-	-	34.92 (3.66)	29.41 (3.85)	2.68 (1.01)	2.19 (0.66)
		MSFA1	BTES	35.77 (3.97)	41.45 (4.26)	44.45 (4.34)	49.68 (4.71)	53.56 (4.27)	44.98 (4.08)	35.36 (3.52)	34.72 (3.57)	1.61 (0.50)	1.74 (0.54)
		Proposed	Proposed	**41.61** (5.09)	**43.99** (5.34)	**51.21** (5.71)	**52.48** (4.87)	**57.92** (4.44)	**49.44** (4.66)	**38.49** (3.71)	**37.59** (3.56)	**1.46** (0.47)	**1.49** (0.49)
D65	CAVE	Bayer	AHD	-	-	-	-	-	-	39.87 (3.85)	38.50 (3.87)	2.55 (1.02)	3.23 (0.90)
		Bayer	LPA	-	-	-	-	-	-	**40.60** (3.70)	39.20 (3.75)	2.44 (0.91)	3.13 (0.85)
		MSFA1	BTES	42.59 (4.43)	42.04 (4.29)	40.90 (4.22)	40.28 (4.41)	40.54 (4.72)	41.27 (4.25)	36.63 (3.88)	36.43 (3.87)	2.67 (1.07)	3.54 (1.14)
		Proposed	Proposed	**45.36** (4.49)	**44.76** (4.70)	**48.06** (4.80)	**44.68** (4.86)	**43.96** (4.82)	**45.36** (4.56)	40.00 (3.86)	**39.38** (3.89)	**2.35** (0.95)	**3.09** (0.87)
D65	Our	Bayer	AHD	-	-	-	-	-	-	36.58 (3.46)	34.99 (3.46)	2.44 (0.87)	2.73 (0.97)
		Bayer	LPA	-	-	-	-	-	-	38.08 (3.48)	36.31 (3.60)	2.07 (0.74)	2.29 (0.76)
		MSFA1	BTES	38.30 (3.99)	40.84 (4.27)	39.72 (4.50)	40.14 (4.80)	39.24 (4.30)	39.65 (4.15)	35.79 (3.57)	35.41 (3.52)	1.86 (0.55)	2.31 (0.70)
		Proposed	Proposed	**43.82** (5.41)	**43.28** (5.61)	**46.57** (5.99)	**42.92** (5.20)	**43.62** (5.19)	**44.04** (5.09)	**39.00** (4.02)	**38.07** (3.92)	**1.56** (0.52)	**1.88** (0.61)
F12	CAVE	Bayer	AHD	-	-	-	-	-	-	36.13 (3.41)	30.63 (3.84)	4.06 (1.59)	3.99 (1.32)
		Bayer	LPA	-	-	-	-	-	-	36.57 (3.35)	30.72 (3.83)	3.97 (1.53)	3.94 (1.29)
		MSFA1	BTES	63.47 (4.21)	51.13 (4.17)	53.00 (4.10)	60.34 (4.25)	64.78 (4.61)	58.54 (4.13)	35.83 (3.43)	34.15 (3.51)	2.48 (0.92)	2.81 (1.00)
		Proposed	Proposed	**68.33** (4.34)	**54.45** (4.32)	**59.56** (4.27)	**64.67** (4.45)	**67.85** (4.24)	**62.97** (4.18)	**38.73** (3.33)	**35.35** (3.63)	**2.43** (0.80)	**2.77** (0.84)
F12	Our	Bayer	AHD	-	-	-	-	-	-	34.64 (3.39)	29.57 (3.26)	3.55 (1.21)	2.71 (0.73)
		Bayer	LPA	-	-	-	-	-	-	35.94 (3.24)	31.15 (3.07)	2.97 (0.94)	2.32 (0.55)
		MSFA1	BTES	59.14 (3.87)	50.10 (4.07)	51.62 (4.30)	59.57 (4.70)	63.39 (4.22)	56.76 (4.02)	36.13 (3.19)	35.78 (3.08)	**1.82** (0.50)	1.85 (0.51)
		Proposed	Proposed	**65.06** (4.42)	**52.48** (4.56)	**57.34** (4.89)	**62.07** (4.46)	**65.10** (3.68)	**60.41** (3.89)	**38.34** (3.04)	**37.28** (2.74)	1.86 (0.46)	**1.81** (0.44)

under the CIE A, CIE D65, and CIE F12 illuminants. In most cases, our proposed MSFA and demosaicking algorithm produces the best results. Especially, our proposed multispectral imaging markedly outperforms conventional color imaging for the CIE A and CIE F12 illuminants because it is difficult to estimate the spectral reflectance images accurately from only three-band images under the non-uniform CIE A and CIE F12 illuminants. Fig. 7 shows the visual comparison of the resultant sRGB images. The lower half of the image shows the corresponding color difference (CIEDE2000 [55]) map, where brighter values represent larger colorimetric errors. These results demonstrate that our proposed MSFA and algorithm reproduces the sRGB images more accurately than the conventional color imaging system does. Fig. 8 shows the visual comparison of the resultant sRGB images for the resolution chart. These results demonstrate that our proposed MSFA and algorithm can generate the image without considerable loss of resolution compared with the Bayer CFA, while the BTES algorithm generates the severely blurred image.

V. PROTOTYPE

We built a one-shot multispectral camera prototype to evaluate the feasibility of our proposed MSFA and demosaicking algorithm in a real hardware setup. Fig. 9 shows the configuration of our multispectral camera prototype. The prototype

| CAVE: Feather (CIE A) | Bayer + AHD | Bayer + LPA | MSFA1 + BTES | Pro. MSFA + Pro. Algo. |

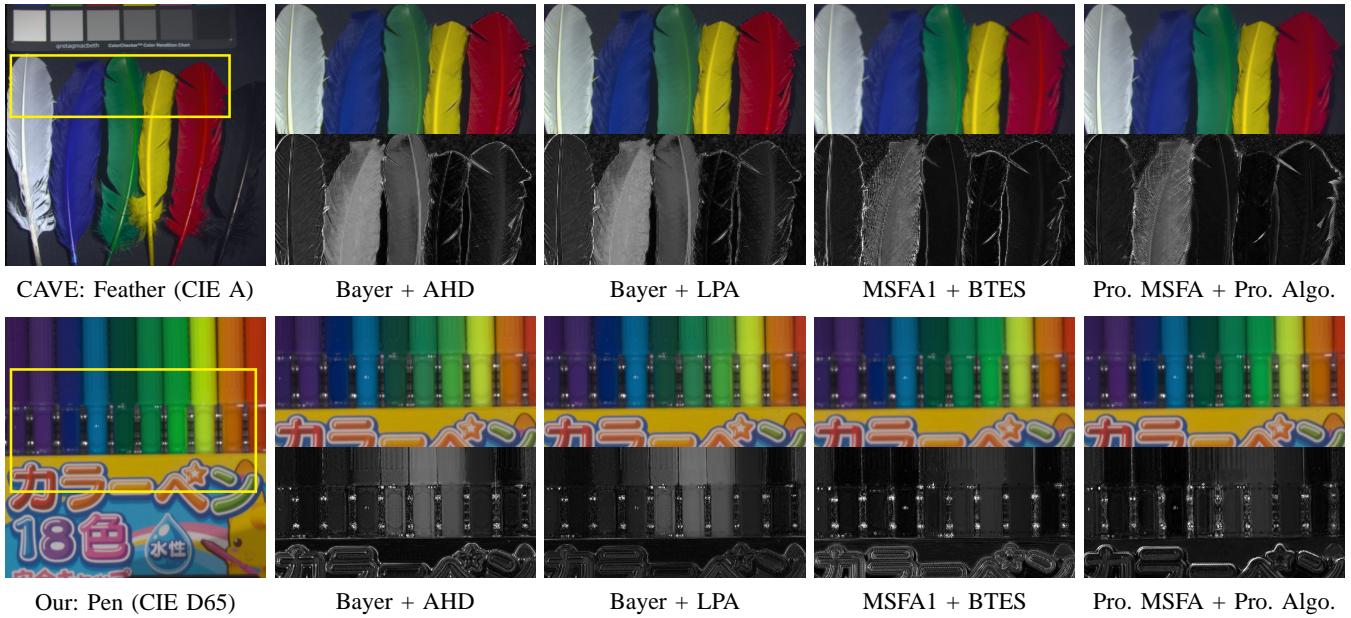| Our: Pen (CIE D65) | Bayer + AHD | Bayer + LPA | MSFA1 + BTES | Pro. MSFA + Pro. Algo. |

Fig. 7. Visual comparison of sRGB images. The lower half of the image shows the color difference (CIEDE2000 [55]) map, where brighter values represent larger colorimetric errors.
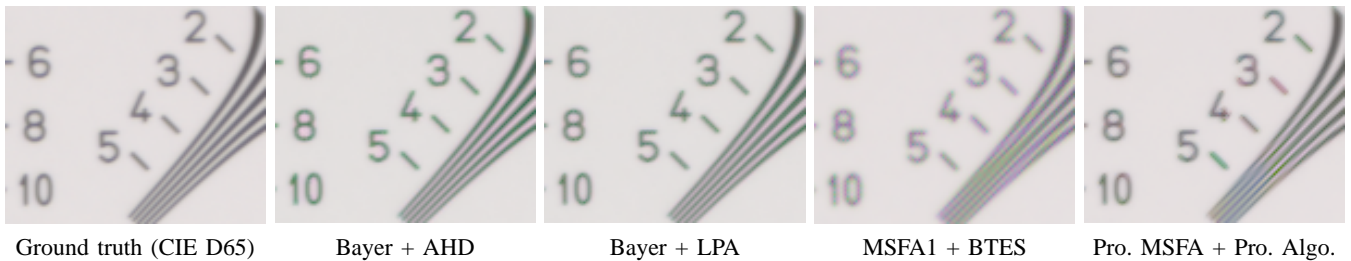

| Ground truth (CIE D65) | Bayer + AHD | Bayer + LPA | MSFA1 + BTES | Pro. MSFA + Pro. Algo. |

Fig. 8. Visual comparison of sRGB images for the resolution chart.
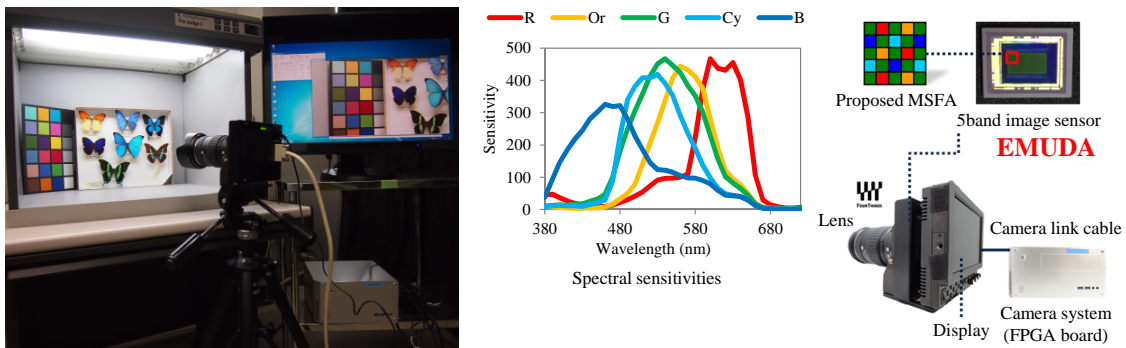
Fig. 9. Configuration of our multispectral camera prototype.

consists of the five-band image sensor (2/3 inch CMOS) and the camera system including a FPGA board, which is linked to the camera by a camera link cable. We named the image sensor Evaluation chip of MUltispectral Demosaicing Algorithm (EMUDA). The EMUDA has our proposed five-band MSFA. We added the Or and Cy bands to conventional RGB bands. Spectral filters of the Or and Cy bands were selected from a set of currently available filters. The camera system executes image processing algorithms including our proposed demosaicking, white balancing, and sRGB transformation. We confirmed that our multispectral camera prototype can capture

a full-HD five-band multispectral video and display the sRGB images at 30 fps without considerable loss of resolution.

We evaluated our prototype for relighting and spectral reflectance estimation. Fig. 10 shows the comparison of relighting results. Fig. 10 (a) is the input image captured by our prototype under a fluorescent illuminant. From the input image, we generated the image under the CIE D65 illuminant by relighting, where the spectral reflectance image is estimated and rendered to the image under the CIE D65 illuminant. Fig. 10 (b) is the relighting result of conventional three-band color imaging, where we only used RGB bands among the
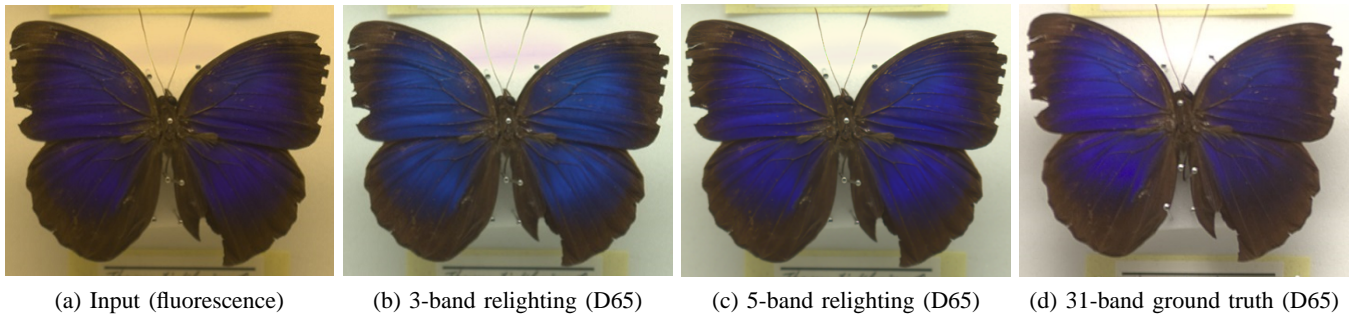
(a) Input (fluorescence) (b) 3-band relighting (D65) (c) 5-band relighting (D65) (d) 31-band ground truth (D65)

Fig. 10. Comparison of relighting results between our proposed five-band multispectral imaging and the conventional three-band color imaging.
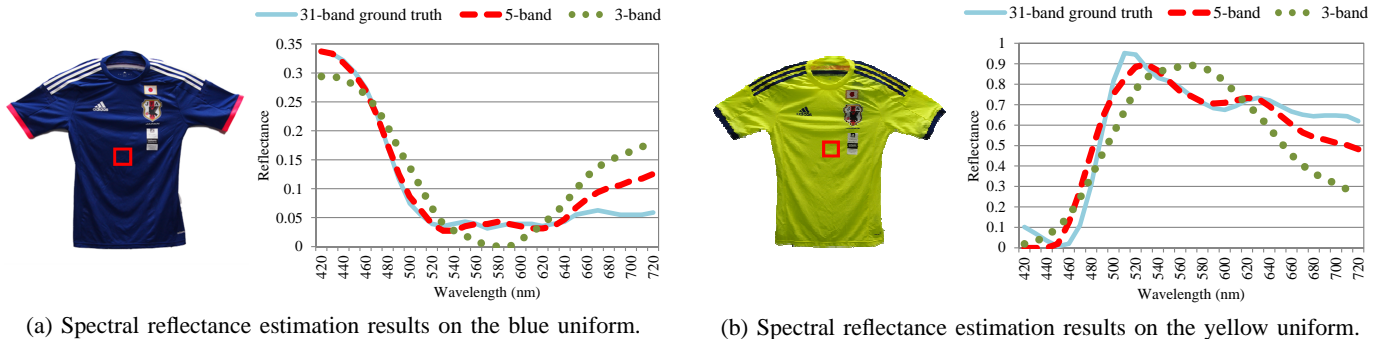

(a) Spectral reflectance estimation results on the blue uniform.

(b) Spectral reflectance estimation results on the yellow uniform.

Fig. 11. Comparison of spectral reflectance estimation between our proposed five-band multispectral imaging and the conventional three-band color imaging.

five bands of our prototype. Fig. 10 (c) is the relighting result of our proposed five-band imaging. Fig. 10 (d) is the ground truth generated from the 31-band multispectral image captured by using the Varispec tunable filter [7], [57]. These results demonstrate that our proposed five-band imaging can relight the image more accurately than the conventional color imaging on the wings of the butterfly.

Fig. 11 shows the comparison of spectral reflectance estimation on the blue and yellow uniforms. The blue line is the 31-band ground truth. The red dash line is the result of using all five bands of our prototype. The green dot line is the result of using only RGB bands of our prototype. Fig. 11 demonstrate that our proposed five-band imaging can estimate the spectral reflectance more accurately than the conventional color imaging.

VI. CONCLUSION

In this paper, we proposed and built the practical one-shot multispectral imaging system using the single image sensor. Our proposed system is based on the joint design of our proposed MSFA and high-performance demosaicking algorithm. In our algorithm, we interpolate each spectral band by the GF [27]. To generate an effective guide image from raw MSFA data, we designed our proposed MSFA based on the density requirement and the derivative requirement. The density requirement ensures the high sampling density of the G band. The derivative requirement ensures the calculation of the adaptive kernel from raw MSFA data. In our algorithm, we first generate the effective guide image from the G band with the high sampling density using the adaptive kernel. Subsequently, we apply the GF to interpolate each spectral

band. From our experiments, we demonstrated that (i) our joint design of the demosaicking algorithm and the MSFA based on the two requirements markedly improves the total performance of the system and (ii) our proposed algorithm outperforms existing algorithms and provides better color fidelity than a conventional color imaging system with the Bayer CFA.

Not only theoretical study, we also built the multispectral camera prototype and confirmed the feasibility of our proposed algorithm and MSFA in an actual hardware setup. Our multispectral camera prototype can capture a full-HD five-band multispectral video and display the sRGB images at 30 fps without significant loss of resolution. We also demonstrated the real applications of our prototype for relighting and spectral reflectance estimation. Our proposed system outperforms the conventional color imaging system especially for objects with highly color-saturated regions.

REFERENCES

[1] A. Ribes, R. Pillay, F. Schmitt, and C. Lahanier, "Studying that smile," *IEEE Signal Processing Magazine*, vol. 25, no. 4, pp. 14–26, 2008.

[2] K. Ohsawa, T. Ajito, H. Fukuda, Y. Komiya, H. Haneishi, M. Yamaguchi, and N. Ohyama, "Six-band HDTV camera system for spectrum-based color reproduction," *Journal of Imaging Science and Technology*, vol. 48, no. 2, pp. 85–92, 2004.

[3] J. Park, M. Lee, M. D. Grossberg, and S. K. Nayar, "Multispectral imaging using multiplexed illumination," *Proc. of IEEE Int. Conf. on Computer Vision (ICCV)*, pp. 1–8, 2007.

[4] X. Cao, H. Du, X. Tong, Q. Dai, and S. Lin, "A prism-mask system for multispectral video acquisition," *IEEE Trans. on Pattern Analysis and Machine Intelligence*, vol. 33, no. 12, pp. 2423–2435, 2011.

[5] X. Cao, X. Tong, Q. Dai, and S. Lin, "High resolution multispectral video capture with a hybrid camera system," *Proc. of IEEE Conf. on Computer Vision and Pattern Recognition (CVPR)*, pp. 297–304, 2011.

[6] R. Shrestha, A. Mansouri, and J. Y. Hardeberg, "Multispectral imaging using a stereo camera: concept, design and assessment," *EURASIP Journal on Advances in Signal Processing*, vol. 57, pp. 1–15, 2011.

[7] J. Y. Hardeberg, F. Schmitt, and H. Brettel, "Multispectral color image capture using a liquid crystal tunable filter," *Optical Engineering*, vol. 41, pp. 2532–2548, 2002.

[8] H. Fukuda, T. Uchiyama, H. Haneishi, M. Yamaguchi, and N. Ohyama, "Development of 16-bands multispectral image archiving system," *Proc. of SPIE*, vol. 5667, pp. 136–145, 2005.

[9] S. Han, I. Sato, T. Okabe, and Y. Sato, "Fast spectral reflectance recovery using DLP projector," *Proc. of Asian Conf. on Computer Vision (ACCV)*, pp. 318–330, 2010.

[10] A. A. Wagadarikar, N. P. Pitsianis, X. Sun, and D. J. Brady, "Video rate spectral imaging using a coded aperture snapshot spectral imager," *Optics Express*, vol. 17, no. 8, pp. 6368–6388, 2009.

[11] R. Habel, M. Kudenov, and M. Wimmer, "Practical spectral photography," *Computer Graphics Forum*, vol. 31, no. 2, pp. 449–458, 2012.

[12] N. Hagen and M. W. Kudenov, "Review of snapshot spectral imaging technologies," *Optical Engineering*, vol. 52, no. 9, pp. 090901 1–23, 2013.

[13] B. Bayer, "Color imaging array," *U.S. Patent 3971065*, 1976.

[14] R. Lukac, *Single-sensor imaging: methods and applications for digital cameras*, CRC Press, 2008.

[15] X. Li, B. Gunturk, and L. Zhang, "Image demosaicing: a systematic survey," *Proc. of SPIE*, vol. 6822, pp. 68221J–1–15, 2008.

[16] B. K. Gunturk, J. Glotzbach, Y. Altunbasak, R. W. Schafer, and R. M. Mersereau, "Demosaicking:color filter array interpolation," *IEEE Signal Processing Magazine*, vol. 22, pp. 44–54, 2005.

[17] D. Menon and G. Calvagno, "Color image demosaicking: An overview," *Signal Processing: Image Communications*, vol. 26, no. 8, pp. 518–533, 2011.

[18] L. Miao and H. Qi, "The design and evaluation of a generic method for generating mosaicked multispectral filter arrays," *IEEE Trans. on Image Processing*, vol. 15, no. 9, pp. 2780–2791, 2006.

[19] L. Miao, H. Qi, R. Ramanath, and W. E. Snyder, "Binary tree-based generic demosaicking algorithm for multispectral filter arrays," *IEEE Trans. on Image Processing*, vol. 15, no. 11, pp. 3550–3558, 2006.

[20] J. Brauers and T. Aach, "A color filter array based multispectral camera," *12. Workshop Farbbildverarbeitung*, 2006.

[21] X. Wang, J. B. Thomas, J. Y. Hardeberg, and P. Gouton, "Median filtering in multispectral filter array demosaicking," *Proc. of SPIE*, vol. 8660, pp. 86600E–1–10, 2013.

[22] F. Yasuma, T. Mitsunaga, D. Iso, and S. K. Nayar, "Generalized assorted pixel camera: postcapture control of resolution, dynamic range, and spectrum," *IEEE Trans. on Image Processing*, vol. 19, no. 9, pp. 2241–2253, 2010.

[23] H. K. Aggarwal and A. Majumdar, "Single-sensor multi-spectral image demosaicing algorithm using learned interpolation weights," *Proc. of IEEE Int. Geoscience and Remote Sensing Symposium (IGARSS)*, pp. 2011–2014, 2014.

[24] G. Baone and H. Qi, "Demosaicking methods for multispectral cameras using mosaic focal plane array technology," *Proc. of SPIE*, vol. 6062, pp. 60620A–1–13, 2006.

[25] Y. Monno, M. Tanaka, and M. Okutomi, "Multispectral demosaicking using adaptive kernel upsampling," *Proc. of IEEE Int. Conf. on Image Processing (ICIP)*, pp. 3218–3221, 2011.

[26] Y. Monno, M. Tanaka, and M. Okutomi, "Multispectral demosaicking using guided filter," *Proc. of SPIE*, vol. 8299, pp. 82990O–1–7, 2012.

[27] K. He, J. Sun, and X. Tang, "Guided image filtering," *IEEE Trans. on Pattern Analysis and Machine Intelligence*, vol. 35, no. 6, pp. 1397–1409, 2013.

[28] K. Hirakawa and T. W. Parks, "Adaptive homogeneity-directed demosaicking algorithm," *IEEE Trans. on Image Processing*, vol. 14, no. 3, pp. 360–369, 2005.

[29] D. Paliy, V. Katkovnik, R. Bilcu, S. Alenius, and K. Egiazarian, "Spatially adaptive color filter array interpolation for noiseless and noisy data," *Int. Journal of Imaging Systems and Technology*, vol. 17, no. 3, pp. 105–122, 2007.

[30] D. Kiku, Y. Monno, M. Tanaka, and M. Okutomi, "Residual interpolation for color image demosaicking," *Proc. of IEEE Int. Conf. on Image Processing (ICIP)*, pp. 2304–2308, 2013.

[31] D. Kiku, Y. Monno, M. Tanaka, and M. Okutomi, "Minimized-Laplacian residual interpolation for color image demosaicking," *Proc. of SPIE*, vol. 9023, pp. 90230L–1–8, 2014.

[32] S. Yamanaka, "Solid state camera," *U.S. Patent 4054906*, 1977.

[33] M. Parmar and S.J. Reeves, "A perceptually based design methodology for color filter arrays," *Proc. of IEEE Int. Conf. on Acoustics, Speech, and Signal Processing (ICASSP)*, vol. 3, pp. 473–476, 2004.

[34] R. Lukac and K. N. Plataniotis, "Color filter arrays: Design and performance analysis," *IEEE Trans. on Consumer Electronics*, vol. 51, no. 4, pp. 1260–1267, 2005.

[35] R. Lukac and K. N. Plataniotis, "Universal demosaicking for imaging pipelines with an RGB color filter array," *Pattern Recognition*, vol. 38, no. 11, pp. 2208–2212, 2005.

[36] A. Hore and D. Ziou, "An edge-sensing generic demosaicing algorithm with application to image resampling," *IEEE Trans. on Image Processing*, vol. 20, no. 11, pp. 3136–3150, 2011.

[37] K. Hirakawa and P. J. Wolfe, "Spatio-spectral color filter array design for optimal image recovery," *IEEE Trans. on Image Processing*, vol. 17, no. 10, pp. 1876–1890, 2008.

[38] L. Condat, "A new color filter array with optimal properties for noiseless and noisy color image acquisition," *IEEE Trans. on Image Processing*, vol. 20, no. 8, pp. 2200–2210, 2011.

[39] J. Gu, P. J. Wolfe, and K. Hirakawa, "Filterbank-based universal demosaicking," *Proc. of IEEE Int. Conf. on Image Processing (ICIP)*, pp. 1981–1984, 2010.

[40] L. Condat, "A generic variational approach for demosaicking from an arbitrary color filter array," *Proc. of IEEE Int. Conf. on Image Processing (ICIP)*, pp. 1625–1628, 2009.

[41] T. Kijima, H. Nakamura, J. Compton, J. Hamilton, and T. E. DeWeese, "Image sensor with improved light sensitivity," *U.S. Patent 7916362*, 2011.

[42] M. Kumar, E. Morales, J. Adams, and W. Hao, "New digital camera sensor architecture for low light imaging," *Proc. of IEEE Int. Conf. on Image Processing (ICIP)*, pp. 2681–2684, 2009.

[43] J. Wang, C. Zhang, and P. Hao, "New color filter arrays of high light sensitivity and high demosaicking performance," *Proc. of IEEE Int. Conf. on Image Processing (ICIP)*, pp. 3214–3217, 2011.

[44] Y. M. Lu, C. Fredembach, M. Vetterli, and S. Süsstrunk, "Designing color filter arrays for the joint capture of visible and near-infrared images," *Proc. of IEEE Int. Conf. on Image Processing (ICIP)*, pp. 3797–3800, 2009.

[45] Z. Sadeghipoor, Y. M. Lu, and S. Süsstrunk, "Correlation-based joint acquisition and demosaicing of visible and near-infrared images," *Proc. of IEEE Int. Conf. on Image Processing (ICIP)*, pp. 3226–3229, 2011.

[46] D. Kiku, Y. Monno, M. Tanaka, and M. Okutomi, "Simultaneous capturing of RGB and additional band images using hybrid color filter array," *Proc. of SPIE*, vol. 9023, pp. 90230V–1–9, 2014.

[47] J. Y. Hardeberg, "Filter selection for multispectral color image acquisition," *Journal of imaging science and technology*, vol. 48, no. 2, pp. 105–110, 2004.

[48] D. Connah, A. Alsam, and J.Y. Hardeberg, "Multispectral imaging: How many sensors do we need?," *Journal of imaging science and technology*, vol. 50, no. 1, pp. 45–52, 2006.

[49] D. Alleysson, S. Süsstrunk, and J. Marguier, "Influence of spectral sensitivity functions on color demosaicing," *Proc. of Color and Imaging Conference (CIC)*, pp. 351–357, 2003.

[50] M. Parmar and S. J. Reeves, "Selection of optimal spectral sensitivity functions for color filter arrays," *IEEE Trans. on Image Processing*, vol. 19, no. 12, pp. 3190–3203, 2010.

[51] Z. Sadeghipoor, Y. M. Lu, and S. Süsstrunk, "Optimum spectral sensitivity functions for single sensor color imaging," *Proc. of SPIE*, vol. 8299, pp. 829904–1–14, 2012.

[52] Y. Monno, T. Kitao, M. Tanaka, and M. Okutomi, "Optimal spectral sensitivity functions for a single-camera one-shot multispectral imaging system," *Proc. of IEEE Int. Conf. on Image Processing (ICIP)*, pp. 2137–2140, 2012.

[53] B. K. Gunturk, Y. Altunbasak, and R. M. Mersereau, "Color plane interpolation using alternating projections," *IEEE Trans. on Image Processing*, vol. 11, no. 9, pp. 997–1013, 2002.

[54] H. Takeda, S. Farsiu, and P. Milanfar, "Kernel regression for image processing and reconstruction," *IEEE Trans. on Image Processing*, vol. 16, no. 2, pp. 349–366, 2007.

[55] G. Sharma, W. Wu, and E. N. Dalal, "The CIEDE2000 color-difference formula: Implementation notes, supplementary test data, and mathematical observations," *Color Research and Application*, vol. 30, no. 1, pp. 21–30, 2005.

[56] "CAVE projects: Multispectral image dataset," http://www.cs.columbia.edu/CAVE/databases/multispectral/.
[57] "Varispec LC tunable filters," http://www.perkinelmer.com/catalog/product/id/varispc.
[58] "CIE: INTERNATIONAL COMMISSION ON ILLUMINATION," http://www.cie.co.at/index.php/LEFTMENUE/DOWNLOADS.
[59] "Useful color data," http://www.cis.rit.edu/research/mcsl2/online/cie.php.
[60] "Color research," http://cs.joensuu.fi/spectral/databases/download/munsell_spec_matt.htm.
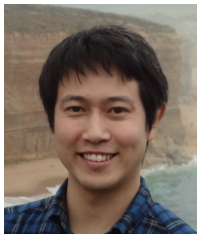
Yusuke Monno received the B.E., M.E., and Ph.D degrees from Tokyo Institute of Technology, Tokyo, Japan, in 2010, 2011, and 2014 respectively. He is currently a postdoctoral researcher at the university. From Nov. 2013 to Mar. 2014, he joined the Image and Visual Representation Group at Ecole Polytechnique Federale de Lausanne, Switzerland, as a research internship student. His research interests are in both theoretical and practical aspects of computer vision and image processing. He is a member of IEEE.

Sunao Kikuchi received the B.E., and M.E. degrees from Hosei University, Tokyo, Japan, in 2006, and 2008 respectively. He is currently a Senior Researcher at Olympus Corporation, where he is engaged in research and development in image processing algorithms at the Research and Development Center. His work focuses on multispectral imaging.

Masayuki Tanaka received his bachelor's and master's degrees in control engineering and Ph.D. degree from Tokyo Institute of Technology in 1998, 2000, and 2003. He joined Agilent Technology in 2003. He was a Research Scientist at Tokyo Institute of Technology since 2004 to 2008. Since 2008, He has been an Associated Professor at the Graduate School of Science and Engineering, Tokyo Institute of Technology. He was a Visiting Scholar with Department of Psychology, Stanford University, CA, USA.

Masatoshi Okutomi received the B.Eng. degree from the Department of Mathematical Engineering and Information Physics, University of Tokyo, Tokyo, Japan, in 1981, and the M.Eng. degree from the Department of Control Engineering, Tokyo Institute of Technology, Tokyo, in 1983. He joined the Canon Research Center, Canon Inc., Tokyo, in 1983. From 1987 to 1990, he was a Visiting Research Scientist with the School of Computer Science, Carnegie Mellon University, Pittsburgh, PA, USA. He received the Dr.Eng. degree from the Tokyo Institute of Technology, in 1993, for his research on stereo vision. Since 1994, he has been with the Tokyo Institute of Technology, where he is currently a Professor with the Department of Mechanical and Control Engineering, Graduate School of Science and Engineering.